HHS Public Access

Author manuscript

Biochemistry. Author manuscript; available in PMC 2022 January 26.

Published in final edited form as:

Biochemistry. 2021 January 26; 60(3): 201–209. doi:10.1021/acs.biochem.0c00834.

Conformational Dynamics of Deubiquitinase A and the Functional Implications

Ashish Kabra, **Ying Li***

Department of Chemistry, University of Louisville, 2320 South Brook Street, Louisville, KY 40208

Abstract

Deubiquitinase A (DUBA) belongs to the ovarian tumor family of deubiquitinating enzymes and was initially identified as a negative regulator of type I interferons, whose overproduction has been linked to autoimmune diseases. The deubiquitinating activity of DUBA is positively regulated by phosphorylation at a single serine residue, S177, which results in minimal structural changes. We have previously shown that phosphorylation induces a two-state conformational equilibrium observed only in the active form of DUBA, highlighting the functional importance of DUBA dynamics. Here, we report the conformational dynamics of DUBA on the microsecond-to-millisecond time scales characterized by NMR relaxation dispersion experiments. We found that motions on these time scales are highly synchronized in both the phosphorylated and nonphosphorylated DUBA. Despite the overall similarity of these two forms, different dynamic properties were observed in the α1 helix and the neighboring regions, including the residue S177, which likely contribute to the activation of DUBA by phosphorylation. Moreover, our data suggest that transient unfolding of the α6 helix drives the global conformational process and that mutations can be introduced to modulate this process, which provides basis for future studies to define the exact functional roles of motions in DUBA activation and substrate specificity.

Graphical Abstract

*To whom correspondence should be addressed: Ying Li, Department of Chemistry, University of Louisville, 2320 South Brook Street, Louisville, KY 40208; ying.li.1@louisville.edu; Tel. (502)852-5975; Fax. (502)852-8149.

Author Contributions

Y.L. conceived the project. A.K. and Y.L. performed the experiments and analyzed data. Y.L. wrote the manuscript.

Supporting Information

The Supporting Information is available free of charge.

Figures S1-S9 and Tables S1-S3 (PDF)

Accession Codes

Deubiquitinase A/OTUD5 (*Homo sapiens*), UniProtKB Q96G74

The authors declare no competing financial interest.

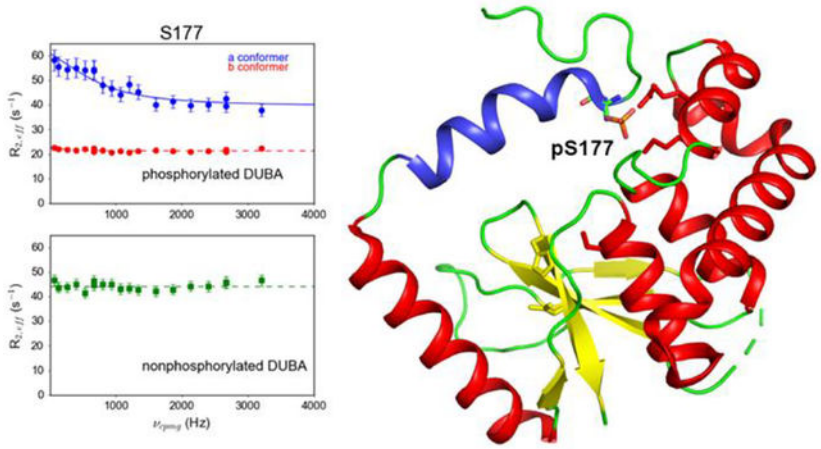

Introduction

Ubiquitination is a pivotal post-translation modification (PTM) that regulates many cellular processes in eukaryotes, including protein degradation, DNA damage responses, protein trafficking, cellular signaling and immune responses.[1, 2] The attachment of monoubiquitin or polyubiquitin chains to target proteins is mediated by a three-enzyme cascade consisting of ubiquitin-activating enzyme (E1), ubiquitin-conjugating enzyme (E2) and ubiquitin ligase (E3). Polyubiquitin chains are built via the formation of an isopeptide or peptide bond between the C- terminus of a ubiquitin and one of the seven lysines (K6, K11, K27, K29, K33, K48, K63) or the N-terminal methionine in another ubiquitin. K48- and K11-linked chains are associated with protein degradation, whereas K63-linked and linear chains are often involved in nondegrative functions such as regulation of cellular signaling cascades.[3] Ubiquitination is reversed by deubiquitinases (DUBs), most of which are cysteine proteases.[4]

Human genome encodes ~100 DUBs, which can be divided into seven families.[5] The activity of DUBs is tightly controlled through diverse mechanisms[6, 7] and aberrant function of DUBs has been linked to human diseases, including cancer, inflammatory and neurodegenerative disorders.[8, 9] In recent years, DUBs have emerged as potential drug targets for both cancer and immune disorders and progress has been made in developing inhibitors selective for specific DUBs.[10] At the molecular level, the activity of DUBs can be regulated by PTMs, the association of accessory domains *in cis* and binding of partner proteins *in trans*.[11] Despite the high prevalence of PTMs, including phosphorylation, ubiquitination, SUMOylation, acetylation, lipidation, glycosylation and oxidation,[6, 12] within the DUB superfamily, the molecular mechanisms of regulation by PTMs are largely unknown. Among all DUBs regulated by phosphorylation, the best studied is deubiquitinase A (DUBA).[11]

DUBA, also named OTUD5, belongs to the ovarian tumor (OTU) family of DUBs, which is the second to the largest and consists of 16 members.[11] Most of OTU DUBs participate in the regulation of cell signaling cascades, such as NF-κB signaling, IRF3 signaling and DNA damage responses.[13, 14] All OTU DUBs are selective for one or two ubiquitin linkages.[13]

DUBA was initially identified as a negative regulator of type I interferons (IFNs) via cleaving K63-linked polyubiquitin chains from tumor necrosis factor receptor-associated factor 3 (TRAF3).[15] Type I IFNs are essential for host antiviral responses,[16] but their overproduction has been linked to autoimmune diseases.[17] Other known functions of DUBA include negative regulation of interleukin-17 production by T cells,[18] attenuation of toll-like receptor 9 (TLR9)-mediated production of anti-inflammatory cytokines,[19] and DNA damage responses.[20] A new role of DUBA in tumorigenesis has been revealed by a recent study.[21] DUBA displays K63- and K48-linkage specificity *in vitro*.[13, 22] The physiological role of the K48-linkage specific cleavage has only recently been revealed by a genetic study showing that DUBA is essential for murine and human development by preventing the degradation of several chromatin regulators.[23]

Enzyme activity of DUBA requires phosphorylation at a single residue, S177, which is located in the disordered region at the N-terminal of the catalytic domain. The crystal structure of the catalytic domain of the phosphorylated DUBA (p-DUBA) conjugated to ubiquitin-aldehyde revealed that the interactions between the phosphate group and the two positively charged residues, R272 and K273, in the α6 helix lead to the enclosure of the C-terminal tail of ubiquitin (Figure 1).[22] NMR studies show that phosphorylation induces minimal structural changes in the apo state of DUBA,[22] raising the question of whether modulation of conformational dynamics plays a role in DUBA activation. Our previous work[24] has shown that several residues in the α1 helix and the neighboring regions display a two-state conformational equilibrium unique to the active form of DUBA. The exchange between the two conformers is slow on the NMR time scales; one conformer is less exposed to solvent and may resemble the crystal structure. In this work, we utilized Carr-Purcell-Meiboom-Gill (CPMG) NMR relaxation dispersion experiments to characterize the conformational dynamics of DUBA in the apo state on the microsecond-to-millisecond (μs-ms) time scales. Our data indicate that the entire DUBA molecule undergoes a global conformational exchange process that involves functionally important structural elements, including the active site. Phosphorylation of S177 modulates the conformational dynamics of the α1 helix and the neighboring regions. Our data provide support for the hypothesis that DUBA undergoes opening and closing motions during the catalytic turnover.[22] The highly synchronized motions may also enable allosteric regulation of DUBA activity by substrates, which is one of the plausible mechanisms for substrate specificity.

Materials and Methods

Sample Preparation and NMR experimental conditions

The construct contains residues 172–344, which corresponds to the catalytic domain of the isoform 2 of DUBA. The plasmid, OTUD5, was a gift from Cheryl Arrowsmith (Addgene plasmid #28270). The R272E/K273E mutant was generated using the mutagenesis service of Genscript. [^{2}H, ^{15}N]-labeled DUBA samples were prepared according to the previously reported methods.[22, 25] The NMR sample buffer contains 50 mM sodium phosphate, pH 7.0, 100 mM NaCl, 1 mM TCEP and 7% D_2O (v/v). All NMR experiments were performed at 298 K unless stated otherwise. The sample temperature was determined using d_4-methanol.[26]

^{1}H CPMG experiments and data analysis

The constant-time amide ^{1}H CPMG experiments were performed at the static magnetic field strength of 16.4 T, using a pulse sequence previously described,[27] on samples containing 580 – 680 μM DUBA. One additional data set was acquired at 14.1 T on a wild-type p-DUBA sample. The experiments were carried out in an interleaved fashion. The constant-time relaxation period was set to 30 ms for wild-type DUBA samples and 34 ms for the K272E/R273E mutant. The optimal lengths of the relaxation period were different because of the faster exchange rates observed on the mutant. The ^{1}H refocusing pulses during the CPMG period was applied at the B_1 field strength of ~25 kHz. Repetition rates of ^{1}H 180° pulses, $\upsilon_{CPMG} = 1/4\tau$, where 2τ is the spacing between adjacent π pulses, range between 66.7 Hz and 3200 Hz for the wild-type samples. The repetition rates range between 117.6 Hz and 3764.7 Hz for the R272E/K273E mutant. Each 2D was recorded with 2048 × 220 complex points, 24 transients and a recycle delay of 1.5 s. The data were processed using NMRPipe[28] and visualized using Sparky.[29] The effective transverse relaxation rates ($R_{2,eff}$) were determined according to the equation $R_{2,eff} = -\frac{1}{T_{relax}}\ln\frac{V(\upsilon_{CPMG})}{V_0}$, where V_0 and $V(\nu_{CPMG})$ are the cross-peak volumes measured without and with the constant-time relaxation period, respectively, and T_{relax} is the length of the constant time period. Cross-peak volumes were determined using the program PINT.[30, 31] The relaxation dispersion profiles were fit to a two-site exchange model under fast-exchange approximation:[32]

$$R_{2,eff} = \frac{\phi_{ex}}{k_{ex}}\left[1 - \frac{4\upsilon_{CPMG}}{k_{ex}}\tanh\left(\frac{k_{ex}}{4\upsilon_{CPMG}}\right)\right] + R_2^0$$

in which R_2^0 is the limiting relaxation rate constant in the absence of exchange broadening; $\phi_{ex} = p_1 p_2 \Delta\omega_{12}^2$, where $\Delta\omega_{12}$ is the chemical shift difference between the two states, and p_1 and p_2 are fractional populations of the two states, respectively; $k_{ex} = k_1 + k_{-1}$, where k_1 and k_{-1} are the rate constants of the forward and reverse conformational transitions, respectively.

Data fitting was performed by minimizing the function χ^2 using the LMFIT python package.[33] Residues that display <35% uncertainty in k_{ex} from individual fitting were selected for group fitting according to the criterion $\chi^2_{\text{group}}/\chi^2_{\text{invididual}} < 2.0$.[34] The rate of transverse relaxation resulting from conformational exchange (R_{ex}) at $\nu_{CPMG} = 0$ was calculated according to $R_{ex} = \frac{p_1 p_2 \Delta\omega_{12}^2}{k_{ex}}$.

^{15}N relaxation experiments

The ^{15}N longitudinal (R_1) and transverse (R_2) relaxation experiments were performed with the standard pulse sequences.[35] In the transverse (R_2) relaxation experiments, the data were recorded in an interleaved fashion with relaxation delays of 10, 30, 50 and 70 ms. ^{15}N 180° refocusing pulses were applied at 1 ms interval. The water magnetization was completely dephased at the beginning of the transverse relaxation period. In the longitudinal (R_1) relaxation experiments, the data were recorded with relaxation delays of 90, 180, 330, 550, 800 and 1050 ms.[36] The Data were processed with NMRPipe.[28] Cross-peak intensities were

determined using Sparky.[29] The data were fit to an exponential function using the curve_fit() function in the SciPy python library.[37]

Results

DUBA undergoes a global conformational process on the microsecond-to-millisecond time scales

Broadening of NMR spectral lines and the resulting low signal intensities are signatures of conformational exchanges on the μs-ms scales.[38] Among ~ 120 cross-peaks detectable in the ^{15}N TROSY spectra of p-DUBA, many display broad ^{1}H lines, whereas the ^{15}N transverse relaxation rates of majority of the resonances are consistent with the molecular weight.[24, 25] TROSY spectra of nonphosphorylated DUBA (np-DUBA) display similar features. The backbone assignments of p-DUBA and np-DUBA are available in the Biological Magnetic Resonance Bank (BMRB) under accession codes 27495 and 27494, respectively. Based on this observation, we performed constant-time amide ^{1}H Carr-Purcell-Meiboom-Gill (CPMG) experiments[27] to characterize the conformational dynamics of both p-DUBA and np-DUBA. In these experiments, the effective transverse relaxation rates ($R_{2,eff}$) were measured during a constant time period, which contains a variable number of equally spaced 180° refocusing pulses. Dependence of $R_{2,eff}$ on the frequency at which the refocusing pulses were applied, termed relaxation dispersion, is an indication of conformational exchange processes. Initial data fitting revealed that the exchange is fast on the NMR time scales and therefore a two-state exchange model at fast-exchange approximation[32] was employed for subsequent data fitting. The use of this model was justified by the quadratic dependence of R_{ex} on the B_0 field strength observed on data at 16.4 T and 14.1 T of a p-DUBA sample (data not shown). F-test ($p = 0.01$) was used to determine whether the data on each residue are fit with the two-state exchange model or the no exchange model where $R_{2,eff}$ is constant. The analysis of CPMG relaxation dispersion profiles allows the kinetic rate constant (k_{ex}) and the contribution of conformational exchange to the transverse relaxation (R_{ex}) to be determined. The square root of R_{ex} is proportional to the chemical shift differences, which reflect the structural differences between the two states. To ensure that the observed relaxation dispersions (Figures S1 and S2) do not result from the exchange between monomer and soluble oligomers, which may form at high concentrations, experiments were also performed on a low concentration p-DUBA sample (100 μM), which yielded data that qualitatively agree with that from samples at a higher concentration (Figure S3). In p-DUBA, ~100 cross-peaks show detectable relaxation dispersions. Individual data fitting yielded similar exchange rates (k_{ex}) of ~5000 s^{-1} for most residues. The data were subsequently group fit with a common exchange rate for residues that satisfy $\chi^2_{group}/\chi^2_{inividual} < 2.0$.[34] Group fitting yielded $k_{ex} = 4954 \pm 82$ s^{-1} for p-DUBA (Table S1). np-DUBA undergoes a similar conformational exchange process with the exchange rate of 5750 ± 110 s^{-1} (Table S2).

R_{ex} measured on p-DUBA were mapped to the crystal structure of p-DUBA conjugated to ubiquitin-aldehyde (Figure 1A).[22] Higher R_{ex} corresponds to larger structural differences between the two states, when the exchange rates and relative populations are the same. NMR signals are not visible when R_{ex} is extremely high. In the regions where NMR signals are

visible, 22 residues that display high R_{ex} values (> 10 s^{-1}) are distributed across almost all secondary structural elements (Figures 1A and S4). ~45 residues are not visible and most are located in the regions spanning α5 to α7 helices, β1-α3 loop and β4-β5 loop (Figures 1A and S4). These highly dynamic elements are functionally important, according to the crystal structure.[22] The α6 helix interacts with the α1 helix to regulate DUBA activity (Figure 1A). The distal ubiquitin (Figure S5) binding interface mainly consists of a helical arm (α5 and α6 helices), the succeeding α6-α7 loop (termed variable loop) and the N-terminal part of the α7 helix (Figure 1B). These elements interact with the C-terminus of ubiquitin, hydrophobic residues L8 and I44, and the surrounding regions. Previous work also suggested the functional roles of the β1-α3 loop (termed Cys loop), which precedes the catalytic cysteine and the β4-β5 loop (termed His loop) in controlling activity and/or substrate linkage specificity in DUBs.[13] The His loop and variable loop are not visible, whereas the Cys loop is partially visible, indicating motions of large amplitudes in these regions. In addition to the large number of highly dynamic surface residues, a significant number of buried residues display high R_{ex} values. Among the ~60 buried residues, 18 residues display R_{ex} higher than 5 s^{-1}. The inset of Figure 1A shows four selected residues that are buried, which connect α4, α5, α6 and α7 helices through sidechain contacts. A network of dynamic residues underlies the synchronized motions observed in both p-DUBA and np-DUBA and explains the similarity in the global conformational dynamics in these two forms.

Differences in the dynamics of p-DUBA and np-DUBA

Our previous work indicates that the presence of an equilibrium between two conformers of the α1 helix and the neighboring regions, which are nearly equally populated, is essential for the activity of p-DUBA.[24] In one conformer (named **a** conformer), the interactions between phosphorylated S177 (pS177) and the two positively charged residues, R272 and K273, in the α6 helix are essential. By contrast, such interactions are not required for the formation of the other conformer, the **b** conformer, which alone is not sufficient for the deubiquitinating activity of DUBA.[24] The α1 helix is flexible and displays low ^{15}N transverse relaxation rates and the two conformers do not show significant differences in the motions on the picosecond-to-nanosecond (ps-ns) time scales.[24] By contrast, the ^{1}H CPMG experiments we performed in this work revealed that the two conformers display different dynamic properties on the μs-ms time scales. The largest difference was observed on pS177, for which the **a** conformer displays large relaxation dispersion, whereas the **b** conformer shows no dispersion (Figure 2A). This suggests that the presence of another conformer of pS177, named the **a'** conformer, which is in fast exchange with the **a** conformer (Figure 2D). The rate of exchange derived from individual fitting is similar to that of the global process and the data can be fit globally, suggesting that the motions of pS177 in the **a** conformer are coupled to other parts of DUBA. Similarly, Y175 and E182 also display conformational exchange in the **a** conformer, whereas the **b** conformer displays flat relaxation dispersion profiles (Figure S1A). By contrast, several residues after a short stretch of alanines (A184-A186), including R187, I188, E189, A190 and M191, display relaxation dispersions in both conformers and the data can be fit globally, suggesting the same exchange rates for the two conformers (Figures 2A and S1A).

We have previously constructed a charge reversal double mutant, R272E/K273E, which remains inactive upon phosphorylation.[24] The backbone assignment was performed on the mutant due to significant perturbations of the amide ^{15}N and ^{1}H chemical shifts.[24] The assignments were deposited to BMRB under the entry number 50686. Figure S6 shows the ^{15}N TROSY spectrum with assignments labeled. Compared to the wild-type, more residues yielded visible NMR signals. The mutations presumably disrupt the interactions between pS177 and the α6 helix. In this mutant, the α1 helix and the neighboring disordered regions (residues 174–192) display only one conformer whose chemical shifts overlap with the **b** conformer in the wild-type.[24] We performed the ^{1}H CPMG experiment on the phosphorylated R272E/K273E mutant (p-R272E/K273E) to compare with the wild-type. In this mutant, all residues N-terminal to the α2 helix display flat relaxation dispersion profiles, except for A185 (Figures 2A and S1). Significant changes in the relaxation dispersion profiles have also been observed in other regions, for example, the α6 helix, which consists of residues 266–273 (Figures 2B, C). For pS177, the relaxation dispersion profile of the only conformer in p-R272E/K273E is highly similar to that of the **b** conformer in wild-type, suggesting that the **b** conformer represents an inactive state. However, for most of the residues, the **b** conformer is not identical to the only conformer in the mutant in terms of dynamic properties, despite the nearly identical backbone chemical shifts. In the **b** conformer, several residues after the short stretch of alanines (A184-A186) display conformational exchange at the same rate as the global process (Table S1), suggesting that the α1 helix is not completely detached from the well-folded domain of DUBA and transient interactions exist; the corresponding residues in the mutant do not display conformational exchange.

Despite the overall similarity in the global conformational process between p-DUBA and np-DUBA, the α1 helix and neighboring regions display detectable differences. Most notably, S177 in np-DUBA shows a flat dispersion profile but elevated $R_{2,eff}$ compared to the **b** conformer in p-DUBA (Figure 2A). The higher $R_{2,eff}$ could result from motions that are too fast to yield relaxation dispersion and/or higher solvent exchange rate in np-DUBA. For most of the other residues N-terminal to the α2 helix, partial quenching of motions by phosphorylation, manifested as smaller R_{ex}, is evident for both conformers or the only conformer (Figure S1). In regions outside the N-terminal segment, p-DUBA and np-DUBA are highly similar (Figure S2). Only one residue, E200, displays more than 2-fold difference in the R_{ex} between p-DUBA and np-DUBA. E200 is spatially close to the α1-α2 loop and similarly show decreased R_{ex} in the p-DUBA compared to np-DUBA. The functional significance of this difference is unclear but E200 is located in a region that presumably binds to the proximal ubiquitin (Figure S5), according to previous structural studies of other OTU DUBs.[13, 39]

Perturbations of structural and dynamic properties observed on the R272E/K273E mutant

R272E/R273E mutant was originally constructed to represent a reference conformational state, where the α1 helix is largely detached from the well-folded domain. However, the mutant displays interesting properties that warrant further investigation. We observed additional cross-peaks in the ^{15}N TROSY spectra, among which 24 can be assigned to specific residues by the standard triple resonance experiments. The catalytic cysteine, C224,

the entire Cys loop except G222, most of the residues in the α5 and α6 helices, and part of the α7 helix become visible. The ^{1}H spectral lines are sharper for most of the residues, indicating significant perturbations of the global conformational process. We analyzed the CPMG data on this mutant by first performing individual fitting and found that the exchange rates vary widely across the molecule, ranging from 2000 s^{-1} to higher than 20,000 s^{-1} (Figures 3A, C and Table S3). Many residues in the α5, α6 and α7 helices show higher k_{ex} compared to that of the global process in the wild-type (Figure 2B, C and Figure 3A, C). Interestingly, the residues remote from the site of mutations, such as the Cys loop and the N-terminal portion of the succeeding α3 helix, which harbors the catalytic cysteine also display elevated k_{ex}, suggesting that the effects of the mutation are not confined to regions neighboring the α6 helix (Figures 3A, B, C and Table S3). The least perturbed region in terms of exchange rates is the α2 helix. In fact, global fitting of data from all residues in this helix showing exchange yields k_{ex} = 5910 ± 160 s^{-1}, similar to the wild-type. Most of these residues still show decrease in R_{ex}, which mainly results from smaller chemical shift differences between the two states or smaller population of the minor conformational state (Figure 3D). Overall, on the μs-ms time scales, the motions of almost all residues were perturbed by the charge reversal mutations and are no longer synchronized. The significant perturbations likely result from breaking two salt bridges, R272-E264 (in the α5-α6 loop) and K273-E284 (in the α7 helix), by the R272E/K273E mutations (Figure 3A). The amino acid sequence of the α6 helix is highly variable among OTU family members with small catalytic domains (Figure S7). In DUBA, the presence of four consecutive residues with positive charges (R272, K273, R274 and K275) in the α6 helix and the succeeding loop destabilizes the helix. Breaking the two stabilizing salt bridges in wild-type DUBA results in higher exchange rates throughout the entire molecule.

To deduce the structural differences between wild-type p-DUBA and p-R272E/K273E, we analyzed the chemical shifts. For p-R272E/K273E mutant, secondary structure prediction from NMR chemical shifts using TALOS-N[40] indicates that the α1, α5 and α6 helices display lower helical content compared to the other helices (Figure S8A). ^{15}N R_1 relaxation rates are elevated in the α1 helix and parts of α2, α5 and α6 helices (Figure S9), indicating higher degree of conformational flexibility on the ps-ns time scales. In wild-type DUBA, the α1 helix also has lower helical content according to the NMR chemical shifts[25] and the ^{15}N relaxation data. For the α5 and α6 helices, the comparison between wild-type and the mutant is hindered by NMR signals largely missing in the wild-type. Only the amide cross-peak of one residue, T267 in the α6 helix, can be assigned with high confidence. The ^{13}Cα and ^{13}Cβ chemical shifts of T267 and the ^{13}Cα chemical shift of the preceding residue, F266, shifted towards the random coil values in the mutant (Figure S8B). No large differences in the ^{13}C chemical shifts were observed for any other residues visible in both the wild-type and the mutant (Figure S8B). Taken together, the data suggest that the α6 helix was destabilized by the mutations, whereas most of the other secondary structural elements remain intact. No data are available to deduce the relative helicity and stability of the α5 helix in the mutant with respect to the wild-type. In contrast to the local changes of the ^{13}C chemical shifts, perturbations of the amide ^{15}N and ^{1}H chemical shifts were observed throughout the entire molecule,[24] which likely result from repacking of secondary structural elements.

Structural characteristics of the minor conformational state

According to the analysis of chemical shifts and ^{15}N relaxation data presented above, the R272E/K273E mutant represents a conformational state where the α5 and α6 helices are partially unfolded and dynamic on the ps-ns time scales, whereas other secondary structural elements remain largely intact. The conformational exchange detected by CPMG experiments typically occurs between a major conformational state, which is highly populated, and a minor state, which is sparsely populated and does not yield visible NMR signals, unless both conformers have similar free energy and are nearly equally populated. Although our data do not allow the determination of relative populations between two states due to the fast exchange rates, we assume that one conformer is more stable than the other in the absence of any evidence for an alternative and equally stable conformer from X-ray crystallographic studies.[22] The more stable conformer is hereafter referred to as the major conformer and the other one as the minor conformer. We hypothesize that the major conformer in the R272E/K273E mutant may partially resemble the minor conformer in the wild-type detected by the CPMG experiments. Under this hypothesis, the amide ^{1}H chemical shift differences between the major and the minor states ($\Delta\omega_{12}$) in the wild-type should be correlated with the chemical shift differences between the major state of the wild-type and that of the mutant (|Δδ| ^{1}H). The latter can be easily obtained from ^{15}N TROSY spectra, whereas the former is proportional to $R_{ex}^{1/2}$. Figure 4 displays the correlation plots of $R_{ex}^{1/2}$ versus |Δδ| ^{1}H. We found high degrees of correlation for residues in the Cys loop, the α3 and α4 helices, the β4 and β5 strands (Figure 4A). These secondary structural elements harbor all three catalytic residues (C224, H334 and N336). This observation suggests that in these regions, transition into the minor conformational state is coupled to the partial unfolding of the α6 helix. The correlation is weak in other regions (Figure 4B), except for the α5-α7 helices for which no clear conclusions can be drawn due to the small number of residues visible in the wild-type (Figure 4C). The lack of correlation is most evident in the α2 helix and the β2-β3 loop, where a significant number of residues show high R_{ex}, whereas the perturbations of amide ^{1}H chemical shifts by mutations are small. Taken together, the R272E/K273E mutations have the overall effects of shifting the major conformer to a state that more resembles the minor state under the assumption that the structure of the minor state is largely not perturbed by the mutations, though the relative populations may change due to the perturbed free energy difference between the two states. This is consistent with the decrease in R_{ex} for almost all residues and the higher k_{ex} in most regions of p-R272E/K273E (Figure 3D). More importantly, in the wild-type DUBA, the motions of several functionally important elements are coupled to the unfolding of the α6 helix, suggesting that the dynamics of these elements can be modulated through changing the stability of the α6 helix.

Discussion

DUBA is a highly dynamic enzyme that undergoes motions on multiple time scales. Previous structural and NMR studies hinted at the functional importance of the motions in DUBA,[22] including our own work that identified a two-state conformational equilibrium unique to the active form of DUBA by NMR spectroscopy.[24] Structural and biochemical studies on other DUBs also suggest the functional relevance of conformational plasticity.

Evidence suggests that the structures of many DUBs in the apo state are heterogeneous[41] and can be modulated by binding of accessary domains,[42, 43] partner proteins,[42–44] substrates,[45, 46] and small-molecule inhibitors,[47] thereby controlling enzyme activity and/or substrate specificity. Recent work on USP7 has also shown that point mutations can shift this DUB from the inactive to an active state, supporting the notion that DUBs can be activated through subtle changes in conformational ensembles.[48] Our previous work on DUBA demonstrated that subtle but functionally important changes in the conformational ensembles can be induced by phosphorylation,[24] which is one of the most prevalent PTMs in the DUB family. Limited knowledge on the effects of PTMs on structure and dynamics has hindered the understanding on how DUBs are regulated by PTMs.

In this work, we characterized the conformational dynamics of DUBA on the μs-ms time scales by ^{1}H CPMG experiments, which allowed us to discern the differences in the dynamic properties between p-DUBA and np-DUBA and those between the two conformers in p-DUBA. Phosphorylation of S177 creates a large conformational barrier between two ensembles of conformers (named **a** and **b**) in slow exchange on the NMR time scales, as we previously observed.[24] Conformer **a** is necessary for the high activity of p-DUBA and may resemble the crystal structure, but the dynamic properties that distinguish the **a** conformer from the **b** conformer had not been well defined. In this work, we observed that the **a** conformer of pS177 transitions between two sub-conformers at a rate of ~5000 s^{-1}, which is much faster than the catalytic turnover rate, whereas the **b** conformer displays no conformational exchange. This transition may allow DUBA to sample both an open conformation necessary for substrate binding, as previously hypothesized based on the crystal structure of p-DUBA conjugated to ubiquitin-aldehyde,[22] and a closed conformation similar to the crystal structure. In np-DUBA, S177 displays a flat relaxation dispersion profile but elevated $R_{2,eff}$, which may result from motions too fast to be detected by the CPMG experiments.

The distinct motions of the α1 helix and the neighboring loops in p-DUBA and np-DUBA, especially the segment around S177, may explain the large difference in activity. Motions in the apo state of enzymes can facilitate substrate binding by enabling transitions into to a binding competent state[49, 50] and can also regulate the catalytic cycle by allowing access to conformational states conducive for catalytic turnover.[51–53] The low activity of np-DUBA likely results from its inability to form a highly productive enzyme-substrate complex rather than low binding affinity to substrates because only 3-fold enhancement in the affinity to the fluorogenic ubiquitin-7-amino-4-methylcoumarin (Ub-AMC) substrate was observed upon phosphorylation, whereas the enhancement in k_{cat} is 300-fold.[24] We can speculate that an important feature of the productive enzyme-substrate complex is that the α1 helix can adopt a closed conformation, as defined by the crystal structure of p-DUBA in the ubiquitin-bound state.[22] The only conformer in np-DUBA lies between the **a** and **b** conformers in terms of structural characteristics according to the relative positions of cross-peaks.[24] This observation indicates that at least in the free state, the α1 helix in np-DUBA adopts a more open conformation than the **a** conformer in p-DUBA. In the enzyme-substrate complex formed from np-DUBA, the α1 helix either cannot adopt a closed conformation or fluctuates rapidly between open and closed conformations. Rapid fluctuations between productive and

non-productive states may increase the rate of substrate release and therefore lower the cleavage rate, as recently demonstrated on the HIV-1 protease.[54]

Functional roles of conformational dynamics have been implied by previous studies on other DUBs.[44, 55] A recent study on the structural basis of the K11-linkage specificity of Cezanne, also named OTUD7B, revealed both structural and dynamic changes in the enzyme during the catalytic cycle, using X-ray crystallography in combination with mass spectrometry-based hydrogen exchange experiments.[45] It was found that the proximal ubiquitin binding site is dynamic and only forms transiently during turnover. The dynamic interactions between this site and the proximal ubiquitin underlie the K11-linkage specificity. In DUBA, the presumed proximal ubiquitin binding site (Figure S5), which involves the His loop and part of the α2 helix, is highly dynamic, suggesting that similar mechanism can be in operation. In addition, the K48 and K63 dual linkage specificity of DUBA may result from the conformational plasticity of the proximal ubiquitin binding site.

Identifying the structural determinants that control the conformational dynamics is a key step towards understanding the functional roles of motions in proteins. By comparing data on the wild-type DUBA and the R272E/K273E mutant, we have deduced that the stability of the α6 helix is an important factor that influences the global conformational dynamics, which is driven by partial unfolding of this helix. Tuning the stability of the α6 helix by mutations can be an effective strategy to modulate the relative populations and the rate of transitions between the two states. Future studies on DUBA mutants with altered dynamic properties and on the various conformational states in the enzymatic cycle will shed light on the detailed mechanisms of DUBA activation and substrate specificities. Our current work provides specific directions for these studies and represents an important step toward understanding how PTMs regulate DUB functions.

Supplementary Material

Refer to Web version on PubMed Central for supplementary material.

ACKNOWLEDGMENT

The work was supported by National Institutes of Health Grant R15GM123391 and by startup funds from University of Louisville.

REFERENCES

[1]. Komander D, and Rape M (2012) The ubiquitin code, Annu. Rev. Biochem 81, 203–229. [PubMed: 22524316]

[2]. Ebner P, Versteeg GA, and Ikeda F (2017) Ubiquitin enzymes in the regulation of immune responses, Crit. Rev. Biochem. Mol. Biol 52, 425–460. [PubMed: 28524749]

[3]. Akutsu M, Dikic I, and Bremm A (2016) Ubiquitin chain diversity at a glance, J. Cell Sci 129, 875–880. [PubMed: 26906419]

[4]. Reyes-Turcu FE, Ventii KH, and Wilkinson KD (2009) Regulation and cellular roles of ubiquitin-specific deubiquitinating enzymes, Annu. Rev. Biochem 78, 363–397. [PubMed: 19489724]

[5]. Clague MJ, Urbe S, and Komander D (2019) Breaking the chains: deubiquitylating enzyme specificity begets function, Nat. Rev. Mol. Cell Biol 20, 338–352. [PubMed: 30733604]

[6]. Leznicki P, and Kulathu Y (2017) Mechanisms of regulation and diversification of deubiquitylating enzyme function, J. Cell Sci 130, 1997–2006. [PubMed: 28476940]

[7]. Sahtoe DD, and Sixma TK (2015) Layers of DUB regulation, Trends Biochem. Sci 40, 456–467. [PubMed: 26073511]

[8]. Heideker J, and Wertz IE (2015) DUBs, the regulation of cell identity and disease, Biochem. J 465, 1–26. [PubMed: 25631680]

[9]. Popovic D, Vucic D, and Dikic I (2014) Ubiquitination in disease pathogenesis and treatment, Nat. Med 20, 1242–1253. [PubMed: 25375928]

[10]. Schauer NJ, Magin RS, Liu X, Doherty LM, and Buhrlage SJ (2020) Advances in discovering deubiquitinating enzyme (DUB) inhibitors, J. Med. Chem 63, 2731–2750. [PubMed: 31682427]

[11]. Mevissen TET, and Komander D (2017) Mechanisms of deubiquitinase specificity and regulation, Annu. Rev. Biochem 86, 159–192. [PubMed: 28498721]

[12]. Kessler BM, and Edelmann MJ (2011) PTMs in conversation: activity and function of deubiquitinating enzymes regulated via post-translational modifications, Cell Biochem. Biophys 60, 21–38. [PubMed: 21480003]

[13]. Mevissen TE, Hospenthal MK, Geurink PP, Elliott PR, Akutsu M, Arnaudo N, Ekkebus R, Kulathu Y, Wauer T, El Oualid F, Freund SM, Ovaa H, and Komander D (2013) OTU deubiquitinases reveal mechanisms of linkage specificity and enable ubiquitin chain restriction analysis, Cell 154, 169–184. [PubMed: 23827681]

[14]. Du J, Fu L, Sui Y, and Zhang L (2020) The function and regulation of OTU deubiquitinases, Front. Med 14, 542–563. [PubMed: 31884527]

[15]. Kayagaki N, Phung Q, Chan S, Chaudhari R, Quan C, O'Rourke KM, Eby M, Pietras E, Cheng G, Bazan JF, Zhang Z, Arnott D, and Dixit VM (2007) DUBA: a deubiquitinase that regulates type I interferon production, Science 318, 1628–1632. [PubMed: 17991829]

[16]. Ivashkiv LB, and Donlin LT (2014) Regulation of type I interferon responses, Nat. Rev. Immunol 14, 36–49. [PubMed: 24362405]

[17]. Hall JC, and Rosen A (2010) Type I interferons: crucial participants in disease amplification in autoimmunity, Nat. Rev. Rheumatol 6, 40–49. [PubMed: 20046205]

[18]. Rutz S, Kayagaki N, Phung QT, Eidenschenk C, Noubade R, Wang X, Lesch J, Lu R, Newton K, Huang OW, Cochran AG, Vasser M, Fauber BP, DeVoss J, Webster J, Diehl L, Modrusan Z, Kirkpatrick DS, Lill JR, Ouyang W, and Dixit VM (2015) Deubiquitinase DUBA is a post-translational brake on interleukin-17 production in T cells, Nature 518, 417–421. [PubMed: 25470037]

[19]. Gonzalez-Navajas JM, Law J, Nguyen KP, Bhargava M, Corr MP, Varki N, Eckmann L, Hoffman HM, Lee J, and Raz E (2010) Interleukin 1 receptor signaling regulates DUBA expression and facilitates Toll-like receptor 9-driven antiinflammatory cytokine production, J. Exp. Med 207, 2799–2807. [PubMed: 21115691]

[20]. de Vivo A, Sanchez A, Yegres J, Kim J, Emly S, and Kee Y (2019) The OTUD5-UBR5 complex regulates FACT-mediated transcription at damaged chromatin, Nucleic Acids Res. 47, 729–746. [PubMed: 30508113]

[21]. Li F, Sun Q, Liu K, Zhang L, Lin N, You K, Liu M, Kon N, Tian F, Mao Z, Li T, Tong T, Qin J, Gu W, Li D, and Zhao W (2020) OTUD5 cooperates with TRIM25 in transcriptional regulation and tumor progression via deubiquitination activity, Nat. Commun 11, 4184. [PubMed: 32826889]

[22]. Huang OW, Ma X, Yin J, Flinders J, Maurer T, Kayagaki N, Phung Q, Bosanac I, Arnott D, Dixit VM, Hymowitz SG, Starovasnik MA, and Cochran AG (2012) Phosphorylation-dependent activity of the deubiquitinase DUBA, Nat. Struct. Mol. Biol 19, 171–175. [PubMed: 22245969]

[23]. Beck DB, Basar MA, Asmar AJ, Thompson J, Oda H, Uehara DT, Saida K, D'Souza P, Bodurtha J, Mu W, Barañano KW, Miyake N, Wang R, Kempers M, Nishimura Y, Okada S, Kosho T, Dale R, Mitra A, Macnamara E, Matsumoto N, Inazawa J, Walkiewicz M, Tifft CJ, Aksentijevich I, Kastner DL, Rocha PP, and Werner A (2020) Regulation of human development by ubiquitin chain editing of chromatin remodelers, bioRxiv doi: 10.1101/2020.01.23.917450.

[24]. Kabra A, Rumpa E, and Li Y (2020) Modulation of conformational equilibrium by phosphorylation underlies the activation of deubiquitinase A, J. Biol. Chem 295, 3945–3951. [PubMed: 32071088]

[25]. Kabra A, Benson CA, and Li Y (2019) Backbone ^{1}H, ^{13}C, ^{15}N resonance assignments of deubiquitinase A in non-phosphorylated and phosphorylated forms, Biomol. NMR Assign 13, 37–42. [PubMed: 30232733]

[26]. Findeisen M, Brand T, and Berger S (2007) A 1H-NMR thermometer suitable for cryoprobes, Magn. Reson. Chem 45, 175–178. [PubMed: 17154329]

[27]. Li Y, Altorelli NL, Bahna F, Honig B, Shapiro L, and Palmer AG 3rd. (2013) Mechanism of E-cadherin dimerization probed by NMR relaxation dispersion, Proc. Natl. Acad. Sci. U.S.A 110, 16462–16467. [PubMed: 24067646]

[28]. Delaglio F, Grzesiek S, Vuister GW, Zhu G, Pfeifer J, and Bax A (1995) NMRPipe: a multidimensional spectral processing system based on UNIX pipes, J. Biomol. NMR 6, 277–293. [PubMed: 8520220]

[29]. Lee W, Tonelli M, and Markley JL (2015) NMRFAM-SPARKY: enhanced software for biomolecular NMR spectroscopy, Bioinformatics 31, 1325–1327. [PubMed: 25505092]

[30]. Niklasson M, Otten R, Ahlner A, Andresen C, Schlagnitweit J, Petzold K, and Lundstrom P (2017) Comprehensive analysis of NMR data using advanced line shape fitting, J. Biomol. NMR 69, 93–99. [PubMed: 29043470]

[31]. Ahlner A, Carlsson M, Jonsson BH, and Lundstrom P (2013) PINT: a software for integration of peak volumes and extraction of relaxation rates, J. Biomol. NMR 56, 191–202. [PubMed: 23657843]

[32]. O'Connell NE, Grey MJ, Tang Y, Kosuri P, Miloushev VZ, Raleigh DP, and Palmer AG 3rd. (2009) Partially folded equilibrium intermediate of the villin headpiece HP67 defined by 13C relaxation dispersion, J. Biomol. NMR 45, 85–98. [PubMed: 19644656]

[33]. Newville M, Stensitzki T, Allen D, and Ingargiola A (2014) LMFIT: Non-linear least-square minimization and curve-fitting for python.

[34]. McDonald LR, Boyer JA, and Lee AL (2012) Segmental motions, not a two-state concerted switch, underlie allostery in CheY, Structure 20, 1363–1373. [PubMed: 22727815]

[35]. Zhu G, Xia Y, Nicholson LK, and Sze KH (2000) Protein dynamics measurements by TROSY-based NMR experiments, J. Magn. Reson 143, 423–426. [PubMed: 10729271]

[36]. Millet O, Loria JP, Kroenke CD, Pons M, and Palmer AG (2000) The static magnetic field dependence of chemical exchange linebroadening defines the NMR chemical shift time scale, J Am. Chem. Soc 122, 2867–2877.

[37]. Virtanen P, Gommers R, Oliphant TE, Haberland M, Reddy T, Cournapeau D, Burovski E, Peterson P, Weckesser W, Bright J, van der Walt SJ, Brett M, Wilson J, Millman KJ, Mayorov N, Nelson ARJ, Jones E, Kern R, Larson E, Carey CJ, Polat I, Feng Y, Moore EW, VanderPlas J, Laxalde D, Perktold J, Cimrman R, Henriksen I, Quintero EA, Harris CR, Archibald AM, Ribeiro AH, Pedregosa F, van Mulbregt P, and SciPy C (2020) SciPy 1.0: fundamental algorithms for scientific computing in Python, Nat. Methods 17, 261–272. [PubMed: 32015543]

[38]. Kleckner IR, and Foster MP (2011) An introduction to NMR-based approaches for measuring protein dynamics, Biochim. Biophys. Acta 1814, 942–968. [PubMed: 21059410]

[39]. Wiener R, Zhang X, Wang T, and Wolberger C (2012) The mechanism of OTUB1-mediated inhibition of ubiquitination, Nature 483, 618–622. [PubMed: 22367539]

[40]. Shen Y, and Bax A (2013) Protein backbone and sidechain torsion angles predicted from NMR chemical shifts using artificial neural networks, J. Biomol. NMR 56, 227–241. [PubMed: 23728592]

[41]. Phillips AH, and Corn JE (2015) Using protein motion to read, write, and erase ubiquitin signals, J. Biol. Chem 290, 26437–26444. [PubMed: 26354440]

[42]. Faesen AC, Luna-Vargas MP, Geurink PP, Clerici M, Merkx R, van Dijk WJ, Hameed DS, El Oualid F, Ovaa H, and Sixma TK (2011) The differential modulation of USP activity by internal regulatory domains, interactors and eight ubiquitin chain types, Chem. Biol 18, 1550–1561. [PubMed: 22195557]

[43]. Faesen AC, Dirac AM, Shanmugham A, Ovaa H, Perrakis A, and Sixma TK (2011) Mechanism of USP7/HAUSP activation by its C-terminal ubiquitin-like domain and allosteric regulation by GMP-synthetase, Mol. Cell 44, 147–159. [PubMed: 21981925]

[44]. Li H, Lim KS, Kim H, Hinds TR, Jo U, Mao H, Weller CE, Sun J, Chatterjee C, D'Andrea AD, and Zheng N (2016) Allosteric activation of ubiquitin-specific proteases by beta-propeller proteins UAF1 and WDR20, Mol. Cell 63, 249–260. [PubMed: 27373336]

[45]. Mevissen TET, Kulathu Y, Mulder MPC, Geurink PP, Maslen SL, Gersch M, Elliott PR, Burke JE, van Tol BDM, Akutsu M, Oualid FE, Kawasaki M, Freund SMV, Ovaa H, and Komander D (2016) Molecular basis of Lys11-polyubiquitin specificity in the deubiquitinase Cezanne, Nature 538, 402–405. [PubMed: 27732584]

[46]. Keusekotten K, Paul, Glockner L, Berthe, Rune, Kulathu Y, Wauer T, Manuela, Gyrd-Hansen M, Krappmann D, Hofmann K, and Komander D (2013) OTULIN Antagonizes LUBAC Signaling by Specifically Hydrolyzing Met1-Linked Polyubiquitin, Cell 153, 1312–1326. [PubMed: 23746843]

[47]. Turnbull AP, Ioannidis S, Krajewski WW, Pinto-Fernandez A, Heride C, Martin ACL, Tonkin LM, Townsend EC, Buker SM, Lancia DR, Caravella JA, Toms AV, Charlton TM, Lahdenranta J, Wilker E, Follows BC, Evans NJ, Stead L, Alli C, Zarayskiy VV, Talbot AC, Buckmelter AJ, Wang M, McKinnon CL, Saab F, McGouran JF, Century H, Gersch M, Pittman MS, Marshall CG, Raynham TM, Simcox M, Stewart LMD, McLoughlin SB, Escobedo JA, Bair KW, Dinsmore CJ, Hammonds TR, Kim S, Urbe S, Clague MJ, Kessler BM, and Komander D (2017) Molecular basis of USP7 inhibition by selective small-molecule inhibitors, Nature 550, 481–486. [PubMed: 29045389]

[48]. Ozen A, Rouge L, Bashore C, Hearn BR, Skelton NJ, and Dueber EC (2018) Selectively modulating conformational states of USP7 catalytic domain for activation, Structure 26, 72–84. [PubMed: 29249604]

[49]. Boehr DD, Nussinov R, and Wright PE (2009) The role of dynamic conformational ensembles in biomolecular recognition, Nat. Chem. Biol 5, 789–796. [PubMed: 19841628]

[50]. Weikl TR, and Paul F (2014) Conformational selection in protein binding and function, Protein Sci. 23, 1508–1518. [PubMed: 25155241]

[51]. Boehr DD, McElheny D, Dyson HJ, and Wright PE (2006) The dynamic energy landscape of dihydrofolate reductase catalysis, Science 313, 1638–1642. [PubMed: 16973882]

[52]. Agarwal PK, Doucet N, Chennubhotla C, Ramanathan A, and Narayanan C (2016) Conformational Sub-states and Populations in Enzyme Catalysis, Methods Enzymol. 578, 273–297. [PubMed: 27497171]

[53]. Ma B, and Nussinov R (2010) Enzyme dynamics point to stepwise conformational selection in catalysis, Curr. Opin. Chem. Biol 14, 652–659. [PubMed: 20822947]

[54]. Deshmukh L, Tugarinov V, Louis JM, and Clore GM (2017) Binding kinetics and substrate selectivity in HIV-1 protease-Gag interactions probed at atomic resolution by chemical exchange NMR, Proc. Natl. Acad. Sci. U.S.A 114, E9855–E9862. [PubMed: 29087351]

[55]. Jupin I, Ayach M, Jomat L, Fieulaine S, and Bressanelli S (2017) A mobile loop near the active site acts as a switch between the dual activities of a viral protease/deubiquitinase, PLos Pathog. 13, e1006714. [PubMed: 29117247]

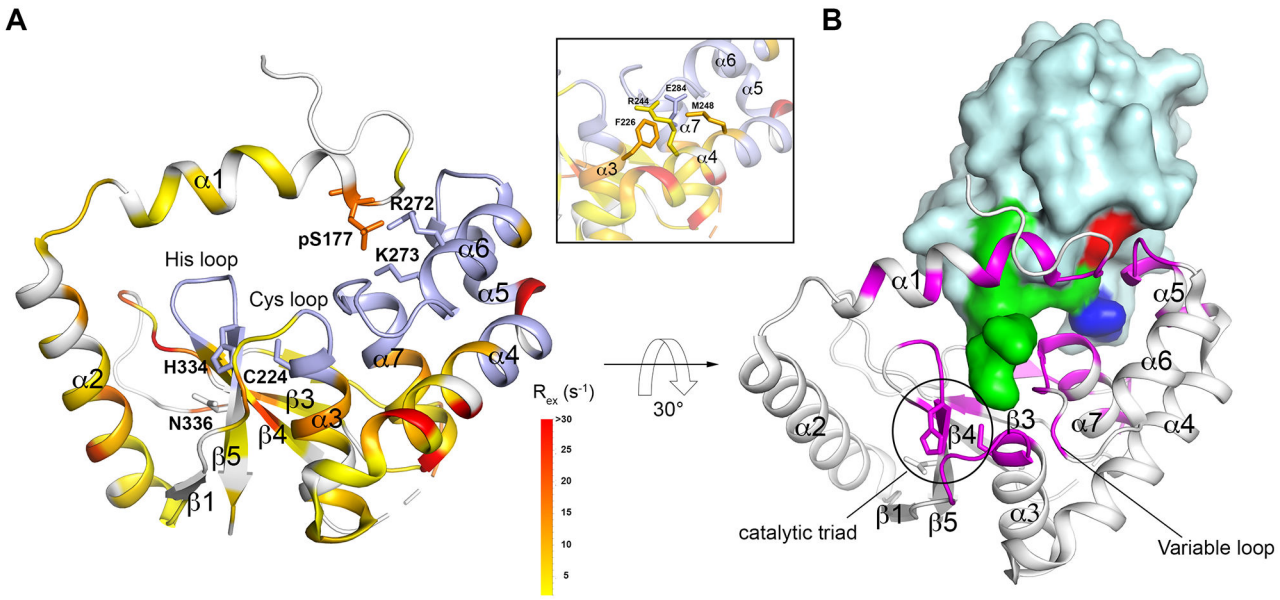

Figure 1.

The crystal structure of DUBA conjugated to ubiquitin-aldehyde (PDB code: 3TMP)[22] (A) R_{ex} mapped to the DUBA structure. Non-proline residues that are not visible in ^{15}N TROSY are colored in light blue. Residues that do not display conformational exchange and proline residues are colored in white. The ubiquitin molecule is not shown. The inset shows four selected residues that are buried and in physical contact, representative of the dynamic core. (B) DUBA structure with the residues within 5 Å from ubiquitin highlighted by magenta. The ubiquitin molecule is shown in surface presentation with the C-terminus (L70 – G76) highlighted in green, I44 highlighted in red and L8 highlighted in blue.

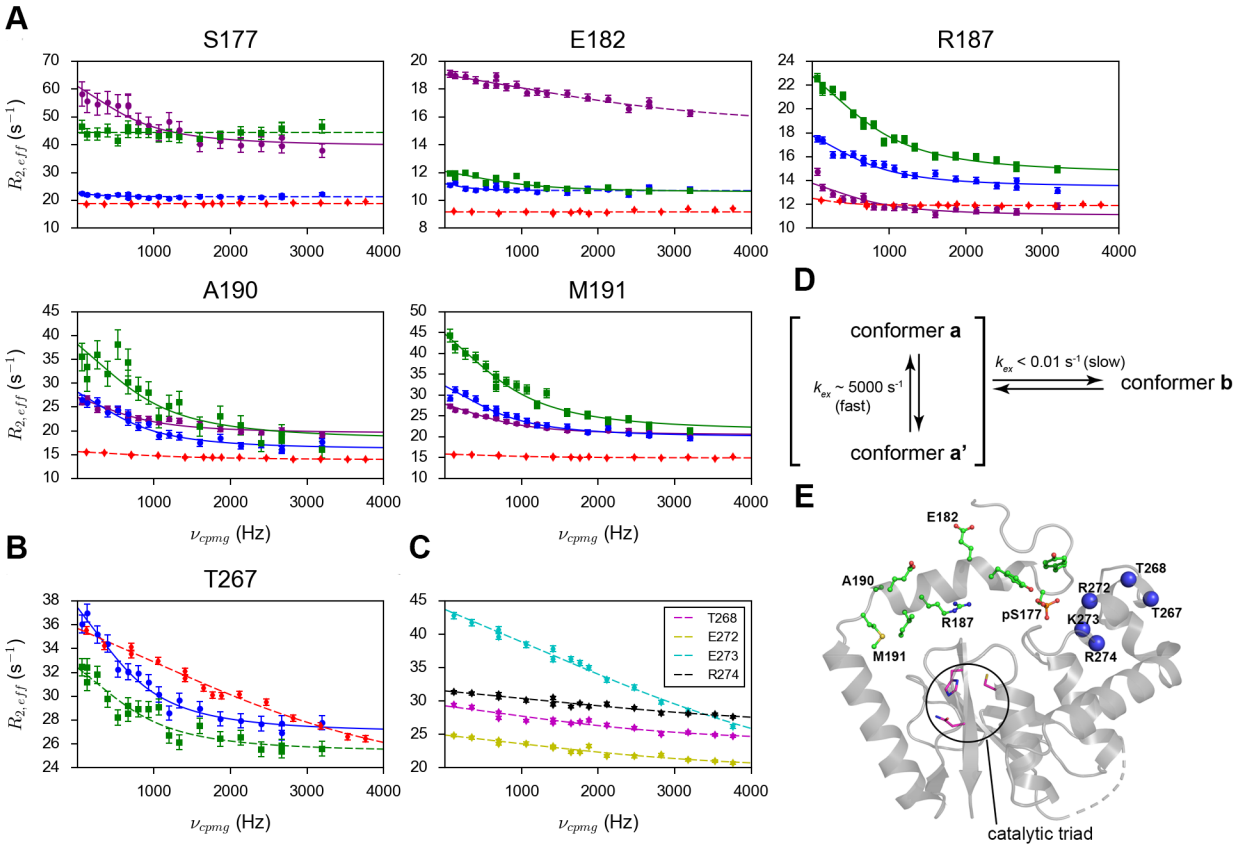

Figure 2.

The amide ^{1}H relaxation dispersion profiles of (A) selected residues in the α1 helix and neighboring disordered regions and (B) T267 from the α6 helix in p-DUBA (**a** conformer in purple; **b** conformer or the only conformer in blue), np-DUBA (green) and p-R272E/K273E mutant (red). (C) The amide ^{1}H relaxation dispersion profiles of other residues in the α6 helix, visible only in the p-R272E/K273E mutant. The solid lines represent group fits and the dashed lines represent individual fits. The uncertainty of $R_{2,eff}$ was determined according to noise. (D) The scheme illustrating the conformational processes of pS177 in the wild-type p-DUBA. (E) Crystal structure of p-DUBA (PDB code: 3TMP) with residues showing two conformers in solution highlighted by the stick-and-ball representation. Blue spheres represent residues in the α6 helix on which CPMG data can be obtained for either the wild-type p-DUBA or the p-R272E/K273E mutant.

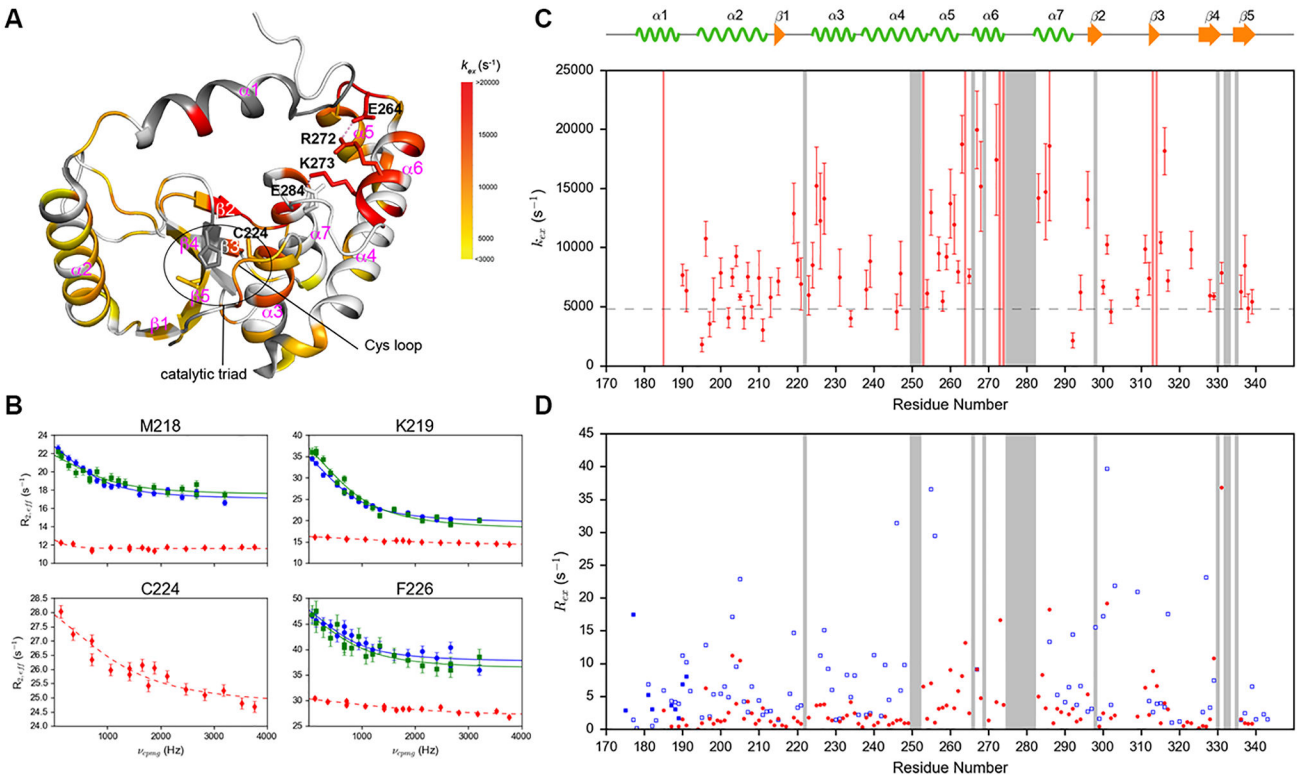

Figure 3.

(A) k_{ex} of 68 residues in p-R272E/K273E mutant mapped to the crystal structure of p-DUBA (PDB code: 3TMP). Dark grey represents residues without conformational exchange. White color represents residues that cannot be assigned or detected, not completely resolved or display higher than 35% uncertainty in k_{ex}. Dash lines represent salt bridges. (B) Selected amide ^{1}H relaxation dispersion profiles of residues in the Cys loop and the α3 helix of p-DUBA (blue), np-DUBA (green) and p-R272E/K273E (red). The solid lines represent group fits and the dashed lines represent individual fits. (C) k_{ex} of p-R272E/K273E plotted as a function of residue number. The dashed line represents the exchange rate of p-DUBA, 4954 s^{-1}. (D) R_{ex} of wild-type p-DUBA (blue) and p-R272E/K273E mutant (red). For p-DUBA, R_{ex} was estimated from the difference in $R_{2,eff}$ at ν_{CPMG} = 66.7 Hz and 3200 Hz; for p-R272E/K273E mutant, R_{ex} was estimated from the difference in $R_{2,eff}$ at ν_{CPMG} = 117.6 Hz and 3764.7 Hz. In both (C) and (D), the regions shaded in grey represent residues without detectable NMR signals in the p-R272E/K273E mutant due to line broadening induced by conformational exchange.

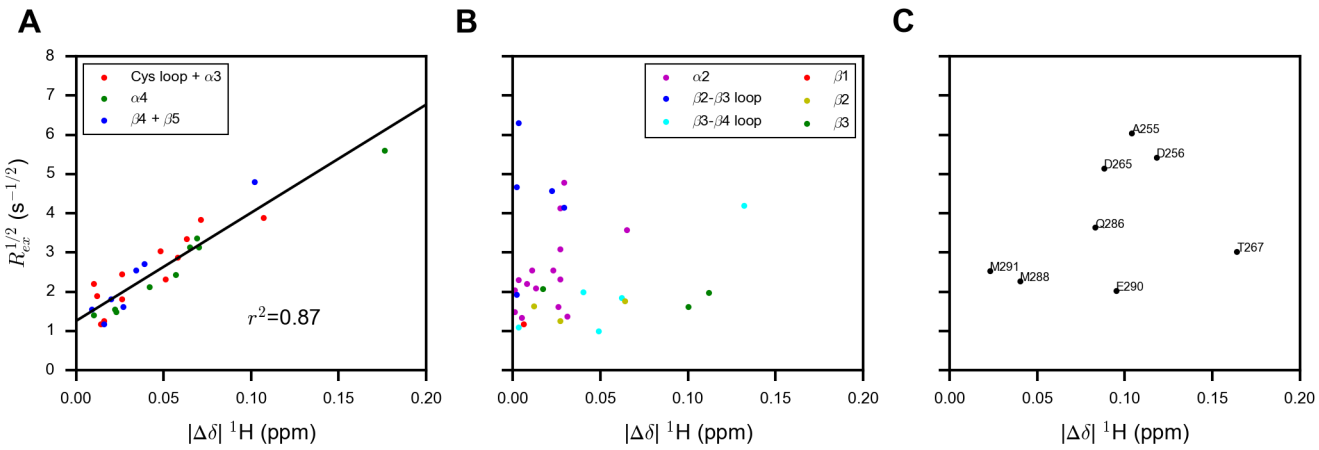

Figure 4.

Correlation plots of $R_{ex}^{1/2}$ from the wild-type p-DUBA versus the absolute value of the amide ^{1}H chemical shift difference between the wild-type p-DUBA and the p-R272E/K273E mutant (|Δδ| ^{1}H) for (A) residues showing good correlations, (B) residues showing poor correlations, and (C) residues located in the α5-α7 helices, which are mostly not visible in the ^{15}N TROSY spectrum of wild-type p-DUBA.